Metallic Nanoalloys on Vertical GaAs Nanowires: Growth Mechanisms and Shape Control of Ni-GaAs Compounds

Nicolas Mallet, Jonas Müller, Julien Pezard, Fuccio Cristiano, Raghda Makarem, Pier-Francesco Fazzini, Aurélie Lecestre, Guilhem Larrieu

Metallic Nano-Alloys on Vertical GaAs Nanowires: Growth Mechanisms and Shape Control of Ni-GaAs compounds.

Nicolas Mallet[1], Jonas Müller[1], Julien Pezard[1], Fuccio Cristiano[1], Raghda Makarem[2], Pier Francesco Fazzini[2], Aurélie Lecestre[1] and Guilhem Larrieu[1*]

[1] LAAS-CNRS, University of Toulouse, CNRS, Toulouse 31031, France

[2] LPCNO, INSA Toulouse, CNRS, University of Toulouse,Toulouse 31077, France

*Corresponding author: Guilhem Larrieu

Email: guilhem.larrieu@laas.fr

Abstract

GaAs nanowires are promising candidates for emerging devices in a broad field of applications (e.g. nanoelectronics, photodetection or photo-conversion). These nanostructures benefit greatly from a vertical integration as it allows for the exhibition of the entire nanowire surface. However, one of the main challenges related to vertical integration is the conception of an efficient method to create low resistive contacts at nano-scale without degrading the device performance. In this paper, we propose a CMOS compatible approach to form alloyed contacts at the extremities of vertical GaAs nanowires. Ni-based and Pd-based alloys on different vertical GaAs nanostructures have been characterized by structural and chemical analysis to identify the phase and to study the growth mechanisms involved at nanoscale. It is shown that the formation of Ni_3GaAs alloy on top of nanowires following the epitaxial relation Ni_3GaAs (0001) ‖ GaAs (111) leads to pyramidal shape with four faces. Finally, guidelines are presented to tune the shape of this alloy by varying the initial metal thickness and nanowire diameters. It will facilitate the fabrication of a nano-alloy structure with tailored shape characteristics to precisely align with a designated application.

Keywords

GaAs nanowires, vertical integration, nano-alloy, Ni-GaAs, Pd-GaAs, interfaces, contacts, solid state reaction.

Introduction

The gallium-arsenide alloy is a well-known III-V semiconductor widely used in photonics and photovoltaic applications. Indeed, its bandgap close to the optimal value of 1.34 eV for single junction solar cell[1] combined with its high electron mobility make it a key material for the future development of the photovoltaics[2,3,4] but also nanoelectronics for amplifier application. In addition, the nanostructuration of the active layer enables to increase the efficiency in applications such as photovoltaics[5,6], CMOS scaling[7,8] or photodetection[9]. In the field of photovoltaic applications, for example, GaAs nanowires have been used to achieve an efficiency beyond the Shockley-Queisser limit[10], a theoretical limit achievable on single junction planar layer. Vertical integration is particularly attractive because of the increased device density[11], higher photon / electrons conversion[12], or improved optoelectronics properties[13,14]. However, the main issue for all these applications is the difficulty to achieve low resistive contacts at the nanoscale.

Historically, gold-based metallic multi-layers are widely used to create low resistive contacts on GaAs: either Ti/Pt/Au on p-GaAs[15,16,17] or Ni/Au/Ge on n-GaAs[15,18,19], both exhibiting a low contact resistivity on GaAs in the range of 10^{-7} Ω.cm^2 to 10^{-6} Ω.cm^2. These layered contacts have two major drawbacks: (i) layer stacking over a nanostructure is often difficult to achieve (ii) contacts containing gold are not compatible with CMOS processes, closing the door to cointegration with standard silicon platforms. Recently, a silicide-like diffusive metallic contact formation technique[20], inspired by the fabrication of silicide contacts used for decades in the silicon industry, showed interesting outcomes. Alloyed contacts based on various metals (Ni, Pd, Co) have been studied on different III-V materials, such as InGaAs, InAs[20,21,22,23] and GaAs[24,25,26,27,28]. Pd based- and Ni based- alloys exhibit interesting low resistive contacts: $2.7 \cdot 10^{-9}$ Ω.cm² on Ni-InAs[29], $1.46 \cdot 10^{-6}$ Ω.cm² on Ni-InGaAs[30], $8.35 \cdot 10^{-5}$ Ω.cm² on Pd-InGaAs

and can be viewed as promising candidates for device integration. However, those results were mainly obtained on bulk substrates. One original study, proposed by Chen et al.[31], focused on the formation of nickelide contacts in vertical InGaAs nano-fins through lateral Ni-diffusion of a neighboring Ni-reservoir. They showed that the formation of $Ni_4InGaAs_2$ on the nanostructured layer is driven by an epitaxial relation between the formed alloy and the InGaAs nanostructure. In such a horizontal configuration, the metal reservoir can be considered as infinite compared to the volume of the semiconducting nanostructure and the contact diffusion is asymmetrical. As depicted in supplementary S1a, the system cannot be considered as perfectly symmetrical, due to the different interfaces (substrate, air) and moreover due to the metal diffusion starting non-homogeneously from one surface of the nanostructure[32,33]. This situation is different when the metallic contact is deposited and formed directly at the top of a nanowire (NW) because the system is perfectly symmetrical and the amount of metal involved in the reaction can be tuned precisely. Normalized by the NW diameter, the reacting amount of metal is exactly the same, whatever the diameter considered (supplementary S1b). In this paper, we develop a dedicated fabrication process for the formation of alloyed contacts on vertical GaAs systems and present a thorough investigation of the contact alloy phase and the growth mechanisms at the nanoscale by coupling X-Ray diffraction (XRD) analysis and Transmission electron microscopy (TEM) combined with Energy-dispersive X-ray spectroscopy (EDX). Ni-GaAs and Pd-GaAs systems have been chosen as test cases and were studied in a planar configuration and in vertical nanowires.

Results

Characterization of planar Ni-GaAs & Pd-GaAs alloys

In order to facilitate phase identification, the formation of Ni-GaAs and Pd-GaAs alloys has been firstly investigated on planar bulk layers. The following experimental protocol was used: First of all, a GaAs wafer is dipped in HCl solution to remove the native oxide just before being loaded in a Physical Vapor Deposition (PVD) chamber (Plassys Nano E-gun) and placed under vacuum. In-situ soft argon milling is performed to remove any remaining surface residues

(amounting to some tens of angstrom on the surface). Then, a 15 nm thick metal layer of Pd or Ni is deposited at 3 nm/min rate. Finally, the alloy formation is activated by rapid thermal annealing (RTA) under a N_2/H_2 gas atmosphere for 1 min at 250°C or 350°C. FIG 1 presents the structural characterization (SEM, TEM) and chemical analysis (XRD) of the formed alloys. A first look on the XRD spectra (FIG 1a) shows that a Ni-GaAs compound is beginning to grow at 250°C. At a higher temperature of 350°C, the peak intensity of the growing phase has increased. The top surface of the alloyed phase is observed by SEM and found to be smooth (FIG 1b). For Pd, we also find a Pd-GaAs phase at 250°C (FIG 1d) which had already started to form at ambient conditions after metal deposition. At higher temperature a second phase appears. The full XRD data for both alloys can be found within the supplementary information S2 & S3. Grains of both interlinked phases can be observed and clearly differentiated by SEM (FIG 1e) due to the associated black and white contrast. TEM cross-section analysis of both layers annealed at 350°C reveals that the entire metal layer has been consumed to form a 31 nm Pd-GaAs alloy or 23 nm of Ni-GaAs alloy. According to Fast Fourier Transform analysis (FFT) of individual grains (FIG 1c), both alloys are polycrystalline (see the red highlighted grain boundaries in FIG 1c & f). The single-phase Ni-GaAs alloy is identified as Ni_3GaAs since the volume ratio between the alloy and the deposited metal is close to 2 [34]. Moreover, the EDX analysis (see S4a for precise results) shows an average atomic ratio for Ni/Ga/As of 57/18/25 (with variations across different grains) which corresponds to Ni_3GaAs stoichiometry[35]. The first phase formed between Pd and GaAs after deposition is likely to be $Pd_{12}Ga_5As_2$ since 3 peaks (marked by the black dashed rectangles) were identified corresponding to the (121), (130) and (040) crystal planes[36] and the atomic ratio of 62/23/15 for Pd/Ga/As measured by EDX is consistent with such a stoichiometry (see S4b). The signal of the (130) peak as-deposited may be broadened due to a superposition with the (111) plane signal of pure Pd. At 350°C, the apparition of a second phase, in addition to the previous one, is identified on the XRD spectrum with 3 new peaks (in green circles). This is additionally highlighted by comparing the SEM images obtained at 250 °C and 350 °C as presented in S5. The exact chemical composition of this phase has not been obtained with enough consistency. In general,

the formation of a second Pd-rich phase has been reported in the literature for T >250°C with a composition close to Pd_4GaAs. The As concentration may however vary[37] due to As surface segregation and desorption close to 400°C which also makes the formation of PdGa possible[38].

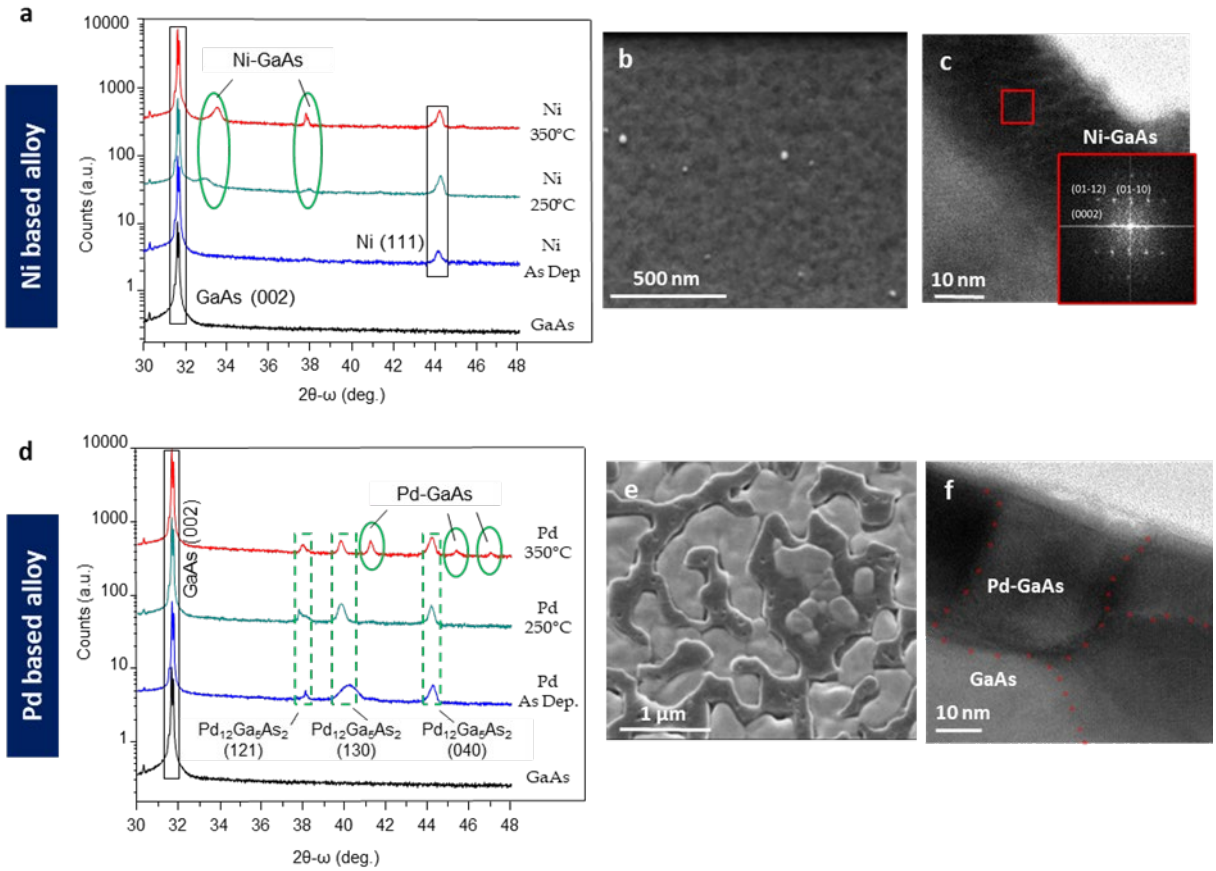

Figure 1: Polycrystalline alloys of 15 nm of Ni or Pd with GaAs after RTA. a) XRD pattern of Ni-GaAs alloy after annealing at 250°C and 350°C. SEM (b) and TEM (c) image of Ni-GaAs formed at 350°C with a measured total thickness of 23 nm. d) XRD pattern of Pd-GaAs alloy after annealing at 250°C and 350°C. As observed by TEM (f), the deposited Pd has completely transformed into Pd-GaAs with a thickness of 31 nm. For 350°C, the formation of a second phase can be observed as a black and white contrast by SEM (e). The crystallinity of individual grains as highlighted by the grain boundaries marked in red (c, f) was verified by FFT as shown in (c).

Formation of nano alloys on vertical GaAs nanowires

In order to reproduce the same analysis strategy on nanoscale contacts, vertical GaAs nanowires have been fabricated by a top-down approach[39] in a 420 nm thick GaAs layer deposited on silicon wafer by metalorganic vapor phase epitaxy (MOVPE)[40]. The grown GaAs layer is free of anti-phase boundaries or point defects. While defects may be present at the nanowire base close to the Si/GaAs interface[39], the GaAs close to the interface with the metallic layer exhibits high crystal quality, as presented in detail in S6.

The full fabrication process is illustrated in S7. Circular nano-masks with diameters between 30 nm and 80 nm have been patterned in a negative resist using electron beam lithography[41] and transferred in the GaAs layer using plasma etching based on a chlorine chemistry. After the resist mask stripping by chemical etching, 5.5 nm of Al_2O_3 is conformally deposited by Atomic Layer Deposition (ALD). The alumina layer is etched by anisotropic RIE on the top and bottom of the nanowires, creating an Al_2O_3 shell on the nanowire's sidewalls. Then, anisotropic metal deposition by PVD and thermal activation are performed as described previously. The alumina shell on the sidewall of the GaAs nanowires (FIG 2a) prevents the diffusion and alloy reaction along the nanowire, preserving the GaAs core.

For the first characterization of the nano-structured alloy formation, the top extremity of the GaAs NW has been selectively etched to create a hollow section of the alumina shell, schematized in FIG 2b, allowing to exactly determine the volume of the successive metal deposition involved in the reaction and to correlate it to the NW diameter (FIG 2c). After annealing at 250°C, the resulting alloys were characterized with SEM, TEM and EDX.

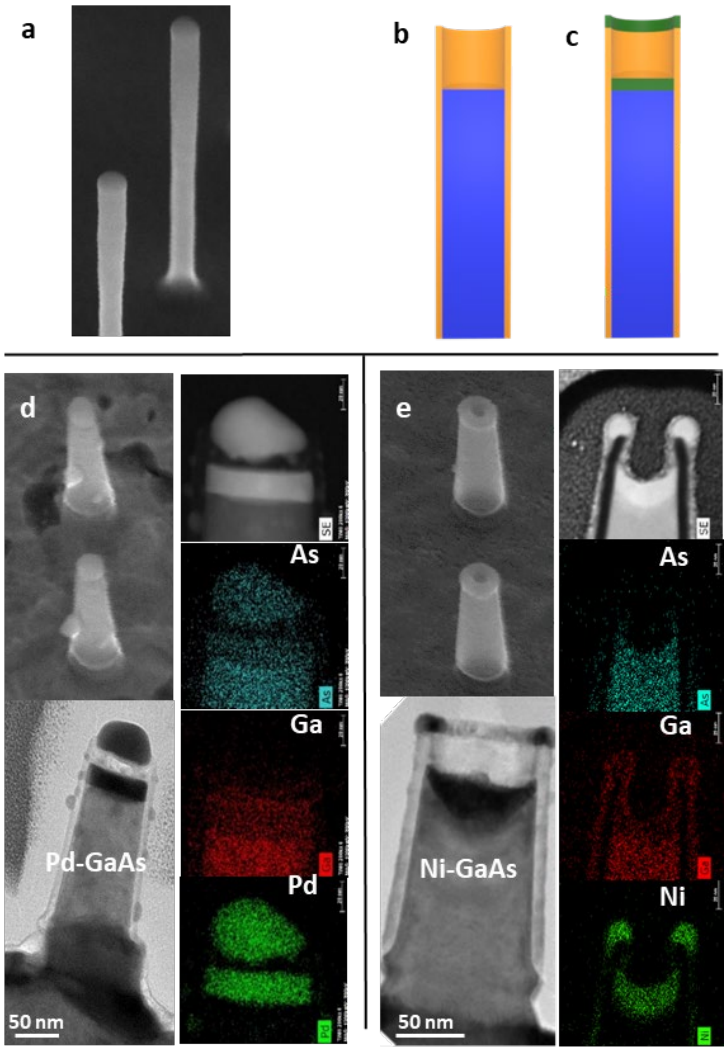

Figure 2: a) SEM image of 220 nm high GaAs nanowires with Al_2O_3 shell. b& c) Schematic representation of the hollowed-out nanowire shell after selective plasma etching and PVD metal deposition. d) SEM, TEM and EDX images of Pd-GaAs (dark) formed inside the shell at the top of the GaAs nanowire. A metallic aggregate made of Pd (≈ 75%) and As (≈ 25%) is located on the top of the structure. e) SEM, TEM and EDX images of Ni-GaAs (dark) formed inside the shell at the top of GaAs.

The Pd has diffused homogeneously into the nanowire, creating a perfectly plane Pd-GaAs alloy interface (FIG 2d). However, an aggregate is formed on top of the nanowire and the alumina shell, separated from the alloyed contact by a void. It is mainly constituted of Pd (≈ 75% atom.) and As (≈ 25% atom.) according to EDX analysis. This aggregate has been found on several types of nanostructures (fins and nanowires) and is specific to palladium (as none was found with nickel alloy). Arsenic found in this aggregate probably comes from its desorption phenomenon occurring during the alloy formation as previously described by Kobayashi et al.[38] and is captured by the unreacted Pd deposited on the alumina rim. The capability of Pd to act as an As-absorber was demonstrated in[42] and reportedly formed Pd_2As

or Pd_8As_3 as a result, of which the later corresponds well to our EDX results. Additionally, we observe the formation of round Pd grains forming on the sidewalls, highlighting the natural tendency of Pd to agglomerate during thermal treatment.

The situation with Ni-based alloy (FIG 2e) looks different: even though Ni is present on the edge of the Al_2O_3 shell, no aggregate is formed from the volume of metal involved in the reaction. As Ni-GaAs alloy formation results in the stable Ni_3GaAs phase within the nanowire, which is confirmed by EDX characterization (see FIG 3b), it is expected that there is no sufficient material desorption to trigger a reaction with the remaining Ni on the edge. It has further been found that the alloy formation was not homogeneous along the nanowire, as it was the case for Pd-based alloy. Instead, a downward pointing conic shape is observed with a thicker part in the center of the nanowire.

Nanowire size dependent growth of Ni-GaAs nano-alloy.

To allow a more detailed investigation a structural analysis has been conducted on nanowires with diameter ranging from 30 nm to 80 nm as presented in FIG 3.

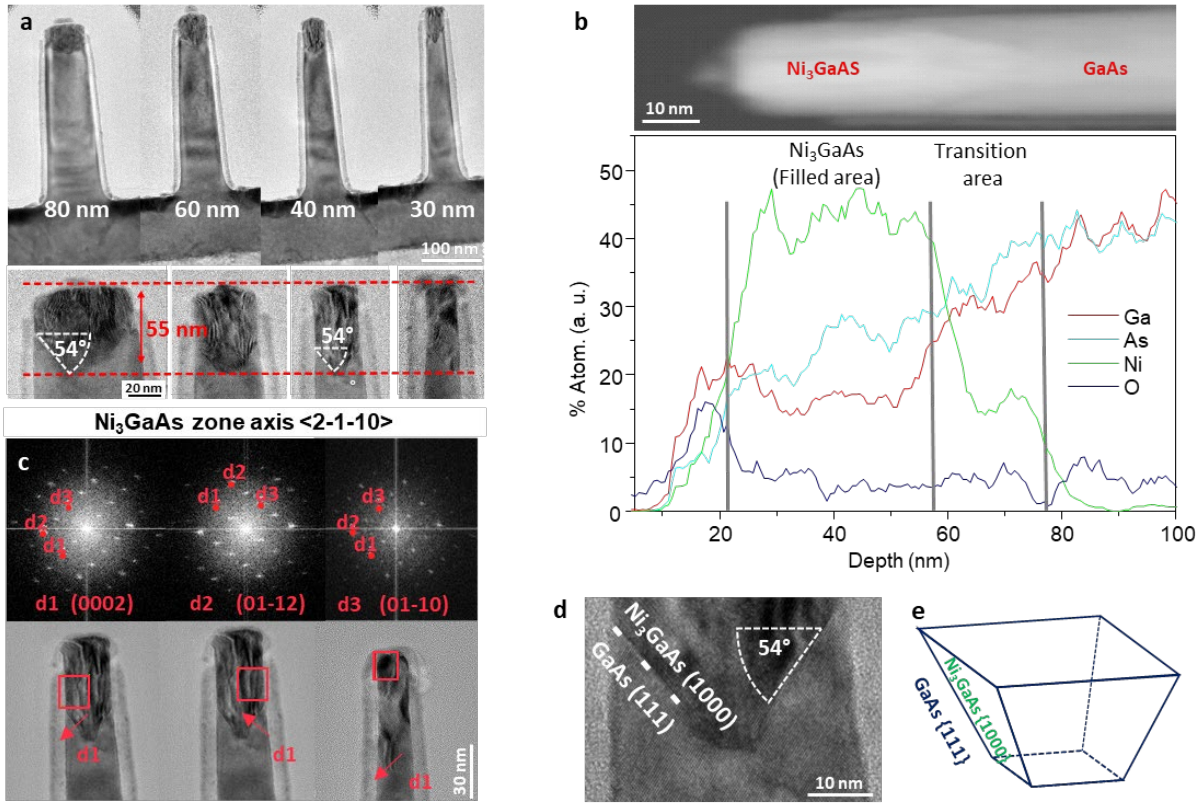

Figure 3: a) TEM image of different GaAs nanowires with Ni_3GaAs alloy at top and bottom. b) EDX scan along the alloy formed on the top end. The detected oxygen comes from Al_2O_3 localized around the alloy. c) Fourier transform applied to TEM images showing the direction of the Ni_3GaAs alloy. The red marks indicate a 90° rotation between both edges of the same nanowire (image on the left and center). d) Zoom on the GaAs (111) plane at the interface with Ni_3GaAs (1000) plane. e) Schematic representation of the crystalline Ni_3GaAs protruding into the nanowires.

From FIG 3a, it appeared that the Ni-based alloy has the same average length (~ 55 nm) independently of the NW diameter. Moreover, the alloy formed on top of nanowires has two distinct regions: (i) bulk contact near the surface: the structure seems to be perfectly cylindrical following the initial NW shape; (ii) transition zone inside the nanowire: the structure is likely to have a square based pyramidal shape. By performing EDX analysis along the NW axis (FIG 3b), these two parts are clearly observable. The cylindrical bulk contact region has an average stoichiometry of 52/19/29 for Ni/Ga/As (variations of ± 3 for Ni, ± 2 for Ga and ± 4 for As). The precision is less compared to previous results from the uniform bulk layer because of the circular geometry and the small diameter of the NW sample. This results in a reduced signal to noise ratio for the analysed materials. Additional fluctuations in the composition stem from the accumulation of gallium at the surface, forming an oxide, while the As concentration depletes near the surface, likely due to desorption.

FFT analysis performed on the HREM images, shown in FIG 3c, are compatible with the structure of a bulk Ni_3GaAs alloy[35]. A complimentary comparison of measured interplanar distances and plane angles is presented in Table S1. TEM images (see FIG 3d) also show a GaAs (111) facet corresponding to a 54° angle. Chen et al.[31] reported a similar observation on Ni alloy formed on horizontal InGaAs nanostructured thin film (50 nm) with epitaxial relation: $Ni_4InGaAs_2$ (0001) ‖ InGaAs (111). In our vertical configuration, it can be stated that the bottom part of the alloy formed on the top extremity is composed of four planes facing equivalent (111) GaAs planes truncated by another plane facing the (100) GaAs plane (FIG 3e). Therefore, a similar epitaxial relation exists on vertical nanowires: Ni_3GaAs (0001) ‖ GaAs (111). Based on reported lattice parameters for both systems[27,43], a small lattice mismatch of -0.98% has been estimated. We found that this epitaxial relation is verified on the nano-alloy (FIG 4a) but also on the bulk alloy layer at the nanowire base (FIG 4b).

To explain this occurrence, the alloy interface with GaAs (100) and GaAs (111) must be compared. Since both epitaxial relations are verified at the nano-scaled contact atop the nanowires as well as for the bulk-like formation at their base, we can determine that the formation energies of those interfaces are close. Otherwise, the interfaces formed during the reaction would be strictly with GaAs (111), as schematized in FIG 4c, 4d.

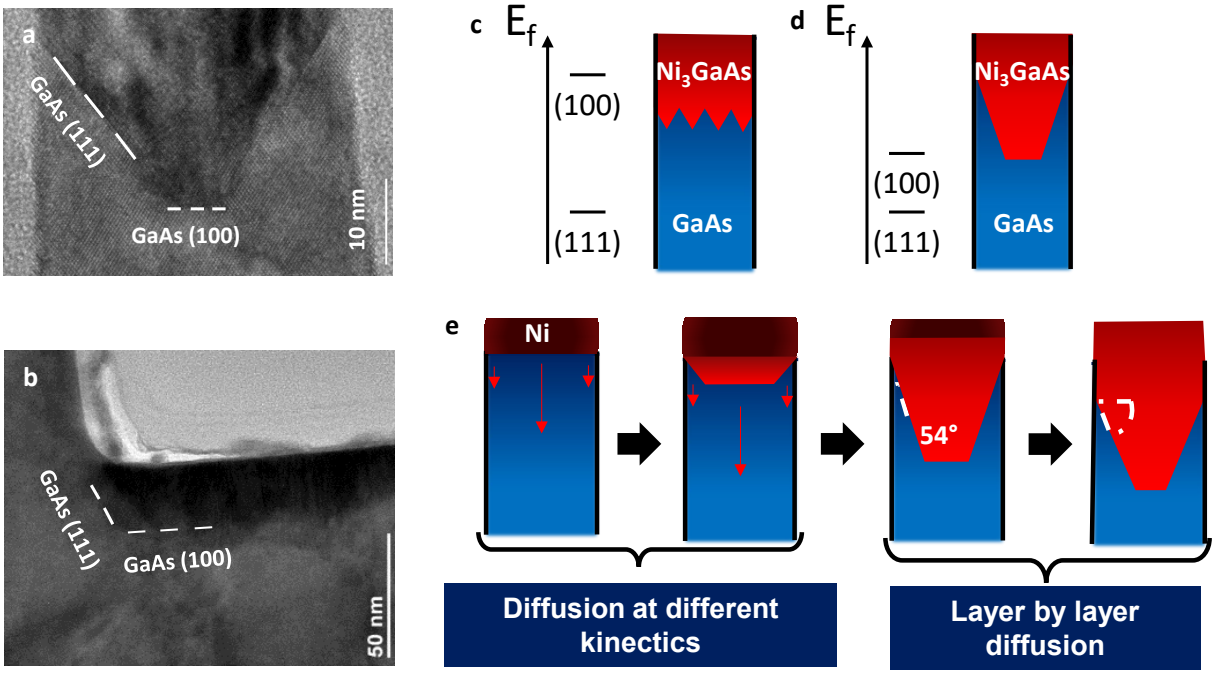

Figure 4: Formation mechanisms for Ni_3GaAs compound on the top of nanowire: TEM images of the actual shape at the top (a) and the bottom (b) of nanowires both presenting the (111) and (100) interface with GaAs. c) Hypothetic shape if only the (111) is stable and d) hypothetic shape if the (100) interface is metastable. e) Proposed growth mechanism in 2 phases: Firstly, diffusion at different kinetics between the center of nanowire, creating a metastable (100), and the triple interface on the edges, creating a non-stable interface. Secondly, after creating the (111) stable interface, layer by layer diffusion leading to the reduction of the (100) interface.

Based on the previous observations, growth mechanisms of the Ni-based nano-alloy are proposed in FIG 4e. The initial diffusion of Ni in the GaAs-matrix has different diffusion kinetics depending on the interfacial relations. Diffusion kinetics are lower at the triple interface ($GaAs/Ni/Al_2O_3$) as suggested by Chen et al. for the $Ni_4InGaAs_2$ alloy formation[31]. It induces an inclined plane between the (100)-GaAs plane formed in the center and the edges of the nanowire. Once this inclined plane aligns with the GaAs (111) plane at 54°, the epitaxial relation is established and the growth mechanism turns into a layer-by-layer diffusion. During this step, this face of the alloy is growing faster relative to the face along GaAs (100), effectively consuming it while decreasing the total interfacial energy. The reaction ends when all the Ni is consumed and its concentration is equilibrated throughout the contact. For limited amounts of Ni, the formation may terminate in an intermediate configuration as observed on the TEM images (e.g. FiG 4a). In the case of small NW diameters (or sufficient Ni being available), the

inclined planes will join to form a perfect pyramid without any observable GaAs (100) plane. The length of the (100) segment *x* as function of the nanowire diameter *d* have been extracted from the TEM images and plotted in FIG 5. A linear numerical fit ($x = 0.36d-5.4$) is obtained with a determination coefficient of $R^2 = 0.986$. A diameter of 15 nm is extrapolated for the completion of a perfect pyramid structure. The shape of the Ni-based nano-alloy can be perfectly mastered by designing the system (t_{Ni}, d) in consequence to get a perfect pyramid shape or to promote a flat interface by minimizing the faceting contribution. This guideline will facilitate the production of a nano-alloy with customizable shape, enabling precise tailoring of its form to align with a specific application.

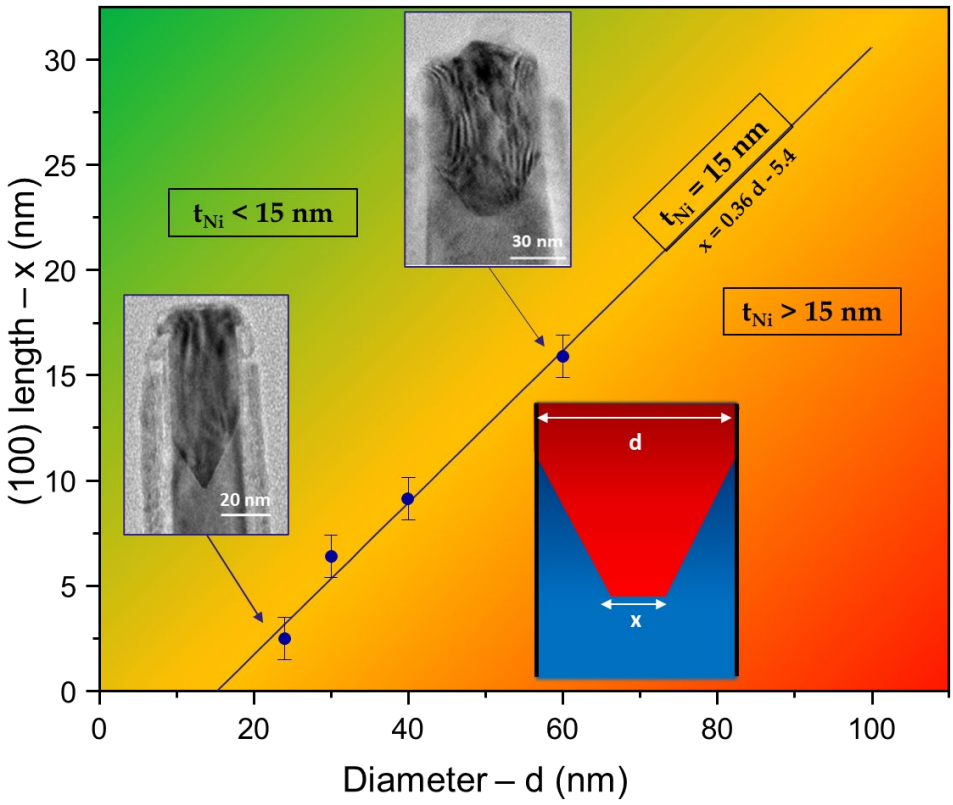

Figure 5: Evolution of the Ni_3GaAs alloy shape with diameter and initial nickel thickness. Experimental measurement performed on TEM images for t_{Ni}=15nm are displayed in blue (scale bar ± 1 nm) and the numerical fit is displayed within the orange zone. By varying the metal thickness for a given NW diameter, the length of the 100 plane may either be increased (green zone) or decreased (red). The observed linear relation on the diameter may however not be valid for vastly different nickel thicknesses.

Conclusion

A detailed study has been proposed to obtain CMOS compatible contacts using palladium and nickel on vertical GaAs nanowires. Firstly, the crystalline structure has been studied: A

polycrystalline Pd-GaAs alloy has been obtained with a $Pd_{12}Ga_5As_2$ phase at 250°C. A new phase interlinked to the previous one appears at higher temperature (350°C), degrading the layer morphology. Moreover, unreacted Pd may absorb out-diffusing As leading to the formation of metal aggregates on top of nanoscale structures which blocks the access to the alloyed contact. The Ni_3GaAs polycrystalline phase formed by RTA is observed to be stable at temperatures of 250°C - 350°C and is found on planar samples as well as on top of nanostructures with diameters down to 25 nm. The alloy formed at nano-scale (top of nanowires) follows a mechanism that can be divided into two steps: the first one is controlled by the difference in diffusion kinetics between the center of the nanowires and its surface boundary. Then, facets with the verified epitaxial relation Ni_3GaAs (0001) ‖ GaAs (111) are formed governed by a layer-by-layer diffusion. Ultimately, the four growing faces will join together as a perfect pyramidal shape. A parameter guideline is proposed to master the shape of the Ni-based nano-alloy in vertical GaAs nanowires depending on the nanowire diameter and the amount of metal involved in the reaction. These results on vertical nanowires can extend the research field on CMOS compatible contacts for improving performance at the device level.

Experimental section

- Sample fabrication:

Used nano-masks are created by e-beam lithography in a Raith-150 e-beam writer. 60 nm thin layers of the negative resist Hydrogen SilsesQuioxane (HSQ) are exposed at an acceleration voltage of 30 kV and an optimized dose of 450 $\mu C/cm^2$. The vertical resist structures are developed in TMAH and rinsed in DI water and methanol.

Vertical GaAs nanowires are created by transferring the HSQ mask using a Sentech Si500 reactive ion plasma (ICP) etching system. Perfectly vertical GaAs nanowires are achieved using a Cl_2/N_2 gas mixture of 9/11 and at 100 W ICP. Remaining resist is stripped by wet-chemical etching in hydrofluoric acid.

The ALD of Al_2O_3 is conducted in a TFS200 system using $Al(CH_3)_3/O_2$ (TMA) precursor and water. Native oxides are removed by dipping in NH_3 (29%) for 1 min. The surface is rinsed and passivated in $(NH_4)_2S$ (20%) for 1 min before being rinsed and dried under N_2. Samples are immediately transferred to the vacuum chamber and the substrate surface de-oxidized by 5 cycles of 500 ms pulsed TMA. The Al_2O_3 is deposited at 300°C during 51 cycles including 500 ms of TMA / 8 s of N_2 / 15 ms of oxygen precursor / 8 s of N_2 per cycle.

Directional etching of the planar alumina layer is achieved by capacitive coupled plasma (CCP) RIE using a Cl_2 and BCl_3 gas mixture in the Sentech SI500. The complete removal of the Al_2O_3 on bulk is confirmed by laser interferometry (DFA) and few seconds of additional etching time are used to remove GaAs at the top of the Al_2O_3 nanowire shell.

Anisotropic physical vapor deposition of Ni or Pd films is performed using a Plassys MEB550SL under vacuum after native oxide removal by dipping in HCl solution, prior to loading, and in-situ soft argon milling. 15 nm thick layers of Pd or Ni are deposited at 3 nm/min. The alloy formation is activated by rapid thermal annealing (RTA) in an AS-One processing furnace under a N_2/H_2 gas atmosphere for 1 min at 250°C for Pd and 300°C for Ni.

- Characterization techniques:

Fabricated structures are observed by scanning electron microscopy (SEM) in a FEI Helios 600i. XRD diffractograms are recorded with a D8-Discover from Bruker using an using a Cu Kα radiation (λ = 0.154 nm) and an incident monochromator Ge(004a). Formed alloys are characterized in detail through transmission electron microscopy (TEM, STEM) and energy dispersive x-ray analysis (EDX) performed in a probe-corrected cold-FEG JEM-ARM200F microscope from JEOL operated at 200 kV. The TEM lamellas are prepared by a focused ion beam (FIB) in a FEI Helios 600i double beam system. A carbon-contrast layer of 50 nm is deposited the structures followed by a Pt layer of more than 500 nm to protect the nanostructures.

Supporting information

Additional illustration of nanowire-contact fabrication configurations; Complimentary XRD diffractograms; Bulk sample EDX results; Pd-GaAs SEM images; STEM and FFT images of vertical GaAs nanowires; Schematic illustration of the complete vertical GaAs nanowire and metallic alloy fabrication process; Comparison of results and literature for interplanar distances and plane angles.

Acknowledgements

The authors wish to thank Thierry Baron from LTM Grenoble for provided the GaAs/Si substrates. This work was supported by Idex UNITI Toulouse (VERTELEC emergence project), by the DGA, by ANR LEGO project and by the French RENATECH network (French national nanofabrication platform).

For Table of Contents Only

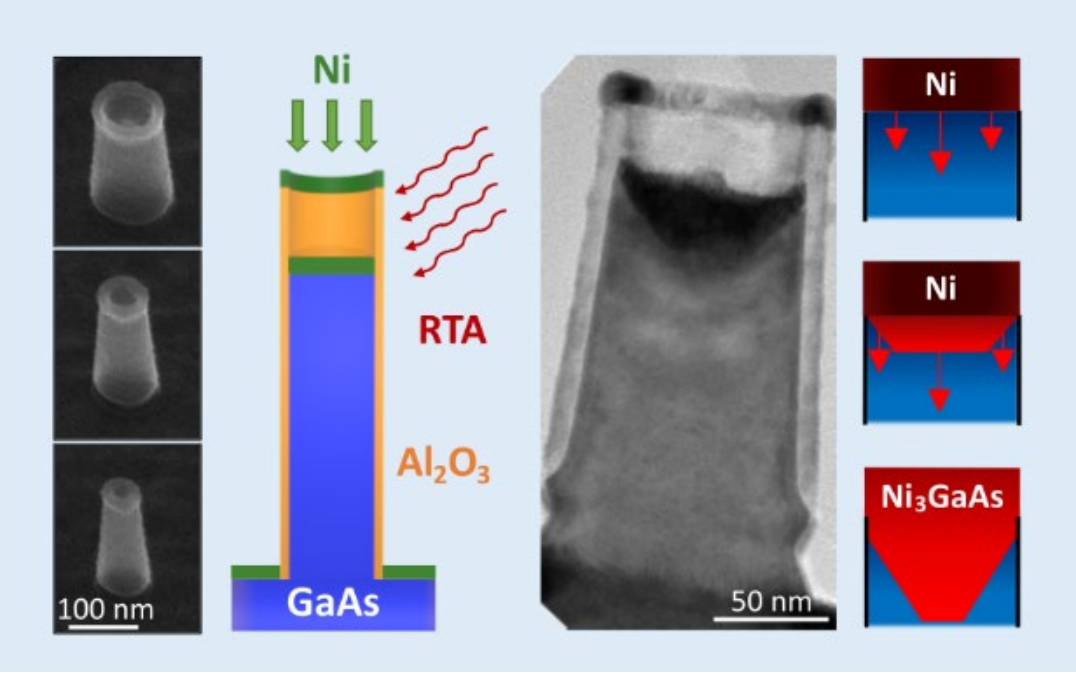

References

[1] Shockley W. ; Queisser H. J. Detailed Balance Limit of Efficiency of p-n Junction Solar Cells *J. Appl. Phys.* **1961**, 32, 510– 519, DOI: 10.1063/1.1736034

[2] Wang X.; Khan M. R.; Gray J. L.; Alam M. A.; Lundstrom M. S. Design of GaAs Solar Cells Operating Close to the Shockley–Queisser Limit *IEEE J. Photovoltaics* **2013**, 3, 737– 744, DOI: 10.1109/JPHOTOV.2013.2241594.
[3] Ataser T.; Akin N.; Ozen Y.; Ozdemir V. Developing of Dual Junction GaInP/GaAs Solar Cell Devices: Effects of Different Metal Contacts *Opt. Quantum Electron.* **2018**, 50, 1– 13, DOI: 10.1007/s11082-018-1546-5
[4] Chen H.-L.; Cattoni A.; De Lépinau R.; Walker A. W.; Höhn O.; Lackner D.; Siefer G.; FaustiniM.; Vandamme N.; Goffard J.; Behaghel B.; Dupuis C.; Bardou N.; Dimroth F.; Collin S. A 19.9%-Efficient Ultrathin Solar Cell based on a 205-nm-thick GaAs Absorber and a Silver Nanostructured Back Mirror *Nat. energy* **2019**, 4, 761– 767, DOI: 10.1038/s41560-019-0434-y
[5] Borgström M. T.; Magnusson M. H.; Dimroth F.; Siefer G.; Hohn O.; Riel H.; Schmid H.; Wirths S.; Bjork M.; Aberg I.; Peijnenburg W.; Vijver M.; Tchernycheva M.; Piazza V.; Samuelson L. Towards Nanowire Tandem Junction Solar Cells on Silicon *IEEE J. Photovoltaics* **2018**, 8, 733– 740, DOI: 10.1109/JPHOTOV.2018.2816264
[6] Valente J.;Godde T.;Zhang Y.; Mowbray D. J.; Liu H. Light Emitting GaAs Nanowires on a Flexible Substrate *Nano Lett.* **2018**, 18, 4206– 4213, DOI: 10.1021/acs.nanolett.8b01100
[7] Guerfi Y.; Larrieu G. Vertical Silicon Nanowire Field Effect Transistors with Nanoscale Gate-All-Around *Nanoscale Res. Lett.* **2016**, 11, 1– 7, DOI: 10.1186/s11671-016-1396-7
[8] Zhao X.; Heidelberger C.; Fitzgerald E. A.; Lu W.; Vardi A.; del Alamo J. A. Sub-10 nm Diameter InGaAs Vertical Nanowire MOSFETs: Ni versus Mo Contacts *IEEE Trans. Electron Devices* **2018**, 65, 3762– 3768, DOI: 10.1109/TED.2018.2859202
[9] Liu W.; Wang W.; Guan Z.; Xu H. Plasmon Modulated Photothermoelectric Photodetector in Silicon Nanostripes *Nanoscale* **2019**, 11, 4918– 4924, DOI: 10.1039/C8NR10222H
[10] Krogstrup P.; Jørgensen H. I.; Heiss M.; Demichel O.; Holm J. V.; Aagesen M.; Nygard J.; Fontcuberta i Morral A. Single-Nanowire Solar Cells beyond the Shockley-Queisser Limit *Nat. Photonics* **2013**, 7, 306– 310, DOI: 10.1038/nphoton.2013.32
[11] Veloso A.; Altamirano-Sánchez E.; Brus S.; Chan B. T.; Cupak M.; Dehan M.; Delvaux C.; Devriendt K.; Eneman G.; Ercken M. Vertical Nanowire FET Integration and Device Aspects *ECS Trans*. **2016**, 72, 31– 42, DOI: 10.1149/07204.0031ecst
[12] Yao M.; Cong S.; Arab S.; Huang N.; Povinelli M. L.; Cronin S. B.; Dapkus P. D.; Zhou C. Tandem Solar Cells Using GaAs Nanowires on Si: Design, Fabrication, and Observation of Voltage Addition *Nano Lett.* **2015**, 15, 7217– 7224, DOI: 10.1021/acs.nanolett.5b03890
[13] Zhang Y.; Wu J.; Aagesen M.; Liu H. III – V Nanowires and Nanowire Optoelectronic Devices *J. Phys. D: Appl. Phys.* **2015**, 48, 463001, DOI: 10.1088/0022-3727/48/46/463001
[14] Tomioka K.; Kobayashi, Y.; Motohisa J. Selective-Area Growth of Vertically Aligned GaAs and GaAs / AlGaAs Core – Shell Nanowires on Si (111) Substrate *Nanotechnology* **2019**, 20, 145302, DOI: 10.1088/0957-4484/20/14/145302
[15] Baca A. G.; Ren F.; Zolper J. C.; Briggs R. D.; Pearton S. J. A Survey of Ohmic Contacts to III-V Compound Semiconductors *Thin Solid Films* **1997**, 308– 309, 599– 606, DOI: 10.1016/S0040-6090(97)00439-2
[16] Piotrowska A. Ohmic Contacts to GaAs: Fundamentals and Practice *Acta Phys. Pol. A* **1993**, 84, 491– 504, DOI: 10.12693/APhysPolA.84.491
[17] Stareev G. Formation of Extremely Low Resistance Ti / Pt / Au Ohmic Contacts to p-GaAs Appl. Phys. Lett. 1993, 62, 2801– 2803, DOI: 10.1063/1.109214
[18] Murakami M. Development of Ohmic Contact Materials for GaAs Integrated Circuits *Mater. Sci. Reports* **1990**, 5, 273– 317, DOI: 10.1016/S0920-2307(05)80006-4
[19] Karbownik P.; Barańska A.; Szerling A.; Macherzyński W.; Papis E.; Kosiel K.; Bugajski M.; Tłaczała M.; Jankiełа R. Low Resistance Ohmic Contacts to n-GaAs for Application in GaAs/AlGaAs Quantum Cascade Lasers *Opt. Appl.* **2009**, 39, 655– 661, URL: https://opticaapplicata.pwr.edu.pl/article.php?id=2009400655
[20] Del Alamo J. A.; Antoniadis D. A.; Lin J.; Lu W.; Vardi A.; Zhao X. Nanometer-Scale III-V MOSFETs *2016 IEEE J. Electron Devices Soc.* **2016**, 4, 205– 214, DOI: 10.1109/JEDS.2016.2571666
[21] Ivana; Kong E. Y.-J.; Subramanian S.; Zhou Q.; Pan J.; Yeo Y.-C. CoInGaAs as a Novel Self-Aligned Metallic Source/Drain Material for Implant-less In0.53Ga0.47As n-MOSFETs *Solid. State. Electron.* **2012**, 78, 62– 67, DOI: 10.1016/j.sse.2012.05.030
[22] Kong E. Y.-J.; Ivana; Zhang X.; Zhou Q.; Pan J.; Zhang Z.; Yeo Y.-C. Investigation of Pd-InGaAs for the Formation of Self-aligned Source/Drain Contacts in InGaAs Metal-Oxide-Semiconductor Field-Effect Transistors *Solid. State. Electron.* **2013**, 85, 36– 42, DOI: 10.1016/j.sse.2013.02.036
[23] Kim S. H.; Yokoyama M.; Taoka N.; Iida R.; Lee S.; Nakane R.; Urabe Y.; Miyata N.; Yasuda T.; Yamada H.; Fukuhara N.; Hata M.; Takenaka M.; Takagi S. Self-aligned Metal Source/Drain $In_xGa_{1-x}As$ n-MOSFETs using Ni-InGaAs Alloy *2010 Int. Electron Devices Meet. IEDM* **2010**, 26.6.1– 26.6.4, DOI: 10.1109/IEDM.2010.5703429
[24] Ogawa M. Alloying Reaction in Thin Nickel Films Deposited on GaAs *Thin Solid Films* **1980**, 70, 181– 189, DOI: 10.1016/0040-6090(80)90426-5
[25] Guérin R.; Guivarc'h A. Metallurgical Study of Ni/GaAs Contacts. I. Experimental Determination of the Solid Portion of the Ni-Ga-As Ternary-phase Diagram *J. Appl. Phys.* **1989**, 66, 2122– 2128, DOI: 10.1063/1.344307
[26] Guivarc'h A.; Guérin R.; Caulet J.; Poudoulec A.; Fontenille J. Metallurgical Study of Ni/GaAs Contacts. II. Interfacial Reactions of Ni Thin Films on (111) and (001) GaAs *J. Appl. Phys.* **1989**, 66, 2129– 2136, DOI: 10.1063/1.344308

[27] Sands T.; Keramidas V. G.; Gronsky R.; Washburn J. Ternary Phases in the Pd-GaAs System: Implications for Shallow Contacts to GaAs *Mater. Lett.* **1985**, 3, 409– 413, DOI: 10.1016/0167-577X(85)90089-8
[28] Olowolafe J. O.; Ho P. S.; Hovel H. J.; Lewis J. E.; Woodall J. M. Contact Reactions in Pd/GaAs Junctions *J. Appl. Phys.* **1979**, 50, 955– 962, DOI: 10.1063/1.326018
[29] Oxland R.; Chang S. W.; Li X.; Wang S. W.; Radhakrishnan G.; Priyantha W.; van Dal M. J. H.; Hsieh C. H.; Vellianitis G.; Doornbos G.; Bhuwalka K.; Duriez B.; Thayne I.; Droopad R.; Passlack M.; Diaz C. H.; Sun Y. C. An Ultralow-Resistance Ultrashallow Metallic Source/Drain Contact Scheme for III-V NMOS *IEEE Electron Device Lett.* **2012**, 33, 501– 503, DOI: 10.1109/LED.2012.2185919
[30] Czornomaz L.;El Kazzi M.; Hopstaken M.; Caimi D.; Mächler P.; Rossel C.; Bjoerk M.; Marchiori C.; Siegwart H.; Fompeyrine J. CMOS Compatible Self-aligned S/D Regions for Implant-free InGaAs MOSFETs *Solid. State. Electron.* **2012**, 74, 71– 76, DOI: 10.1016/j.sse.2012.04.014
[31] Chen R.; Dayeh S. A. Size and Orientation Effects on the Kinetics and Structure of Nickelide Contacts to InGaAs Fin Structures *Nano Lett.* **2015**, 15, 3770– 3779, DOI: 10.1021/acs.nanolett.5b00327
[32] Katsman A.; Yaish Y.; Rabkin E.; Beregovsky M. Surface Diffusion Controlled Formation of Nickel Silicides in Silicon Nanowires *J. Electron. Mater.* **2010**, 39, 365– 370, DOI: 10.1007/s11664-009-1071-1
[33] Katsman A.; Beregovsky M.; Yaish Y. E. Formation and Evolution of Nickel Silicide in Silicon Nanowires *IEEE Trans. Electron Devices* **2014**, 61, 3363– 3371, DOI: 10.1109/TED.2014.2342502
[34] Rabhi S.; Perrin-Pellegrino C.; Zhiou S.; Benoudia M. C.; Texier M.; Hoummada K. Phase Formation between Ni Thin Films and GaAs Substrate *Scr. Mater.* **2017**, 141, 28– 31, DOI: 10.1016/j.scriptamat.2017.07.011
[35] Zheng X.-Y.; Lin J.-C.; Swenson D.; Hsieh K.-C.; Chang Y. A. Phase Equilibria of Ga-Ni-As at 600 °C and the Structural Relationship between γ-Ni_3Ga_2, γ'-$Ni_{13}Ga_9$ and T-Ni_3GaAs *Mater. Sci. Eng. B* **1989**, 5, 63– 72, DOI: 10.1016/0921-5107(89)90308-5
[36] El-Boragy M.; Schubert K. On the Mixtures PdZnMGeN PdAlMSiN PdGaMSiN PdAlMGeN and PdGaMAsN *International Journal of Materials Research* **1981**, 72, 279– 282, DOI: 10.1515/ijmr-1981-720411
[37] Sands T.; Keramidas V. G.; Yu A. J.; Yu K. M.; Gronsky R.; Washburn J. Phase Formation Sequence in the Pd-GaAs System *MRS Online Proceedings Library (OPL)* **1985**, 54, 367– 372, DOI: 10.1557/PROC-54-367
[38] Kobayashi A.; Sakurai T.; Hashizume T.; Sakata T. An Atomistic Study of the GaAs-Pd Interface *J. Appl. Phys.* **1986**, 59, 3448– 3453, DOI: 10.1063/1.336813
[39] Lecestre A.; Martin M.; Cristiano F.; Baron T.; Larrieu G. Large-Scale Monolithic Fabrication of III–V Vertical Nanowires on a Standard Si(100) Microelectronic Substrate *ACS Omega* **2022**, 7, 7, 5836–5843, DOI: 10.1021/acsomega.1c05876
[40] Alcotte R.; Martin M.; Moeyaert J.; Cipro R.; David S.; Bassani F.; Ducroquet F.; Bogumilowicz Y.; Sanchez E.; Ye Z.; Bao X. Y.; Pin J. B.; Baron T. Epitaxial Growth of Antiphase Boundary Free GaAs Layer on 300 mm Si (001) Substrate by Metalorganic Chemical Vapour Deposition with High Mobility *APL Mater.* **2016**, 4, 046101, DOI: 10.1063/1.4945586
[41] Guerfi Y.; Carcenac F.; Larrieu G. High Resolution HSQ Nanopillar Arrays with Low Energy Electron Beam Lithography *Microelectron. Eng.* **2013**, 110, 173– 176, DOI: 10.1016/j.mee.2013.03.055
[42] Uffalussy K. J.; Miller J. B.; Howard B. H.; Stanko D. C.; Yin C.; Granite E. J. Arsenic Adsorption on Copper-Palladium Alloy Films *Ind. Eng. Chem. Res.* **2014**, 53, 7821– 7827, DOI: 10.1021/ie404447b
[43] Lahav A.; Eizenberg M.; Komem Y. Interfacial Reactions between Ni Films and GaAs *J. Appl. Phys.* **1986**, 60, 991– 1001, DOI: 10.1063/1.337343